Supporting Information

Pure silica-supported transition metal catalysts for the non-oxidative dehydrogenation of ethane: Confinement effects on the stability

Sudipta De,[1] Antonio Aguilar-Tapia,[2] Samy Ould-Chikh,[1] Andrea Zitolo,[3] Jean-Louis Hazemann,[2] Genrikh Shterk,[1] Adrian Ramirez,[1] Jorge Gascon*,[1]

[1]KAUST Catalysis Center (KCC), King Abdullah University of Science and Technology, Thuwal 23955, Saudi Arabia

[2]Institut Neel, UPR 2940 CNRS − Université Grenoble Alpes, F-38000 Grenoble, France

[3]Synchrotron SOLEIL, L'orme des Merisiers, 91192 Gif-sur-Yvette, France

Corresponding author email: jorge.gascon@kaust.edu.sa

Table S1. Metal contents in the catalysts determined by ICP analysis

Sample	Theoretical loading during synthesis (wt%)	Actual loading by ICP analysis (wt%)	M/Si (atom %)
V/MFI	0.4	0.39	0.46
Cr@MFI	0.8	0.42	0.49
Fe/MFI	0.5	0.45	0.49
Co@MFI	0.4	0.48	0.49
Ni/MFI	0.5	0.51	0.52
Ga/MFI	0.6	0.56	0.48
Mo/MFI	0.8	0.77	0.49
Pt@MFI	1.6	1.49	0.47
K-Co@MFI	0.4	0.45 (1.04)[a]	0.46 (1.62)[a]
Co/MFI	0.5	0.47	0.48
Co@MFI	1.2	1.31	1.35
Co@MFI	2.2	2.49	2.60
Co/SBA-15	0.5	0.51	0.52
Co/SiO_2	0.5	0.47	0.48

[a]Content of potassium (K) is given in the parentheses.

Table S2. Gibbs energy values of reduction of metal oxides (with stable lowest oxidation state of metal) to metals at 650 °C

Reaction	ΔG_r (kJ mol^{-1})[a]
$VO + H_2 \rightarrow V + H_2O$	153.1
$Cr_2O_3 + 3H_2 \rightarrow 2Cr + 3H_2O$	305.0
$FeO + H_2 \rightarrow Fe + H_2O$	14.8
$CoO + H_2 \rightarrow Co + H_2O$	−28.1
$NiO + H_2 \rightarrow Ni + H_2O$	−41.1
$Ga_2O_3 + 3H_2 \rightarrow 2Ga + 3H_2O$	196.9
$MoO_2 + 2H_2 \rightarrow Mo + 2H_2O$	26.0
$PtO_2 + H_2 \rightarrow Pt + 2H_2O$	−556.0

[a]Calculated by using the standard Gibbs energy data from literature.[1]

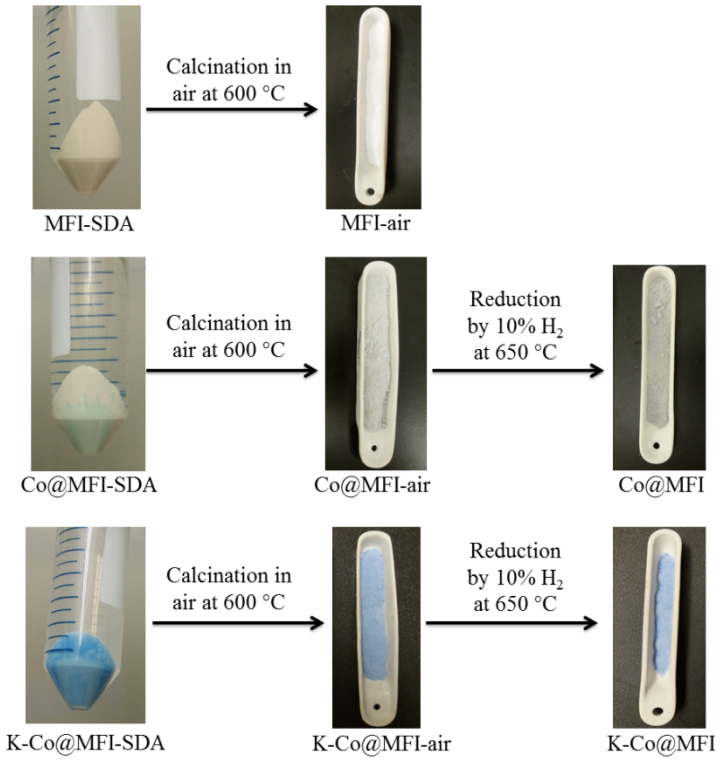

Fig. S1 MFI materials at different stages. SDA is the surface directing agent (TPAOH here). Co loading is 0.5 wt% and K loading is 1 wt%.

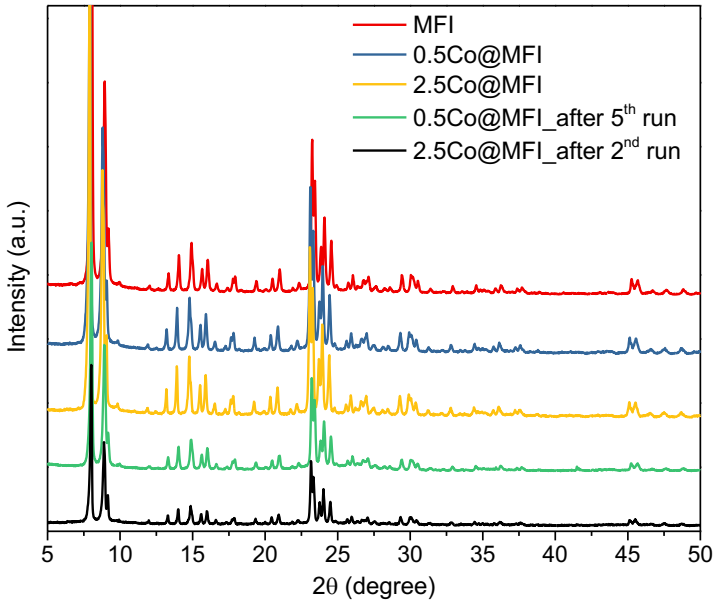

Fig. S2 Powder XRD patterns of fresh and used catalysts.

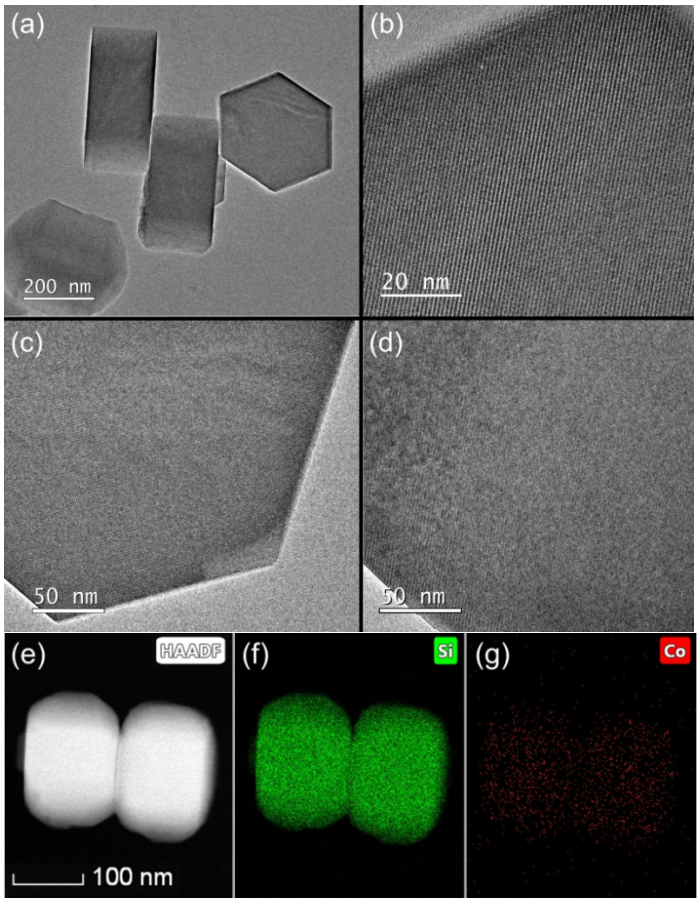

Fig. S3 TEM images of (a) MFI, (b) 0.5Co@MFI, (c) 1.3Co@MFI, and (d) 2.5Co@MFI. (e) STEM-HAADF image and (f, g) elemental mappings of 0.5Co@MFI.

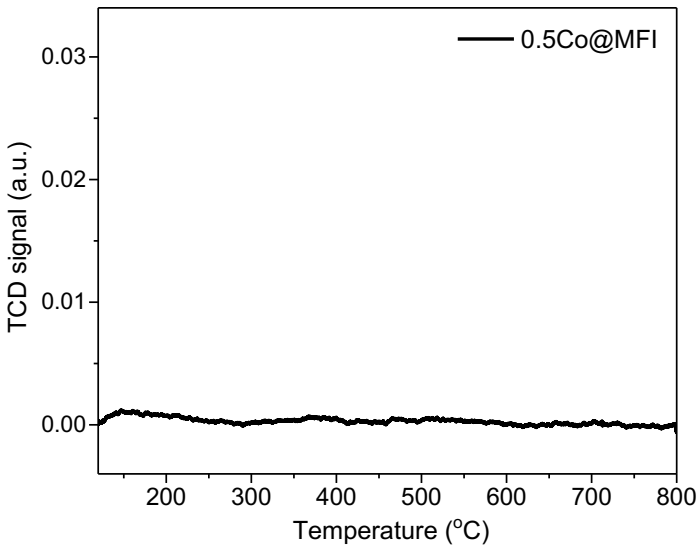

Fig. S4 NH_3-TPD profile of 0.5Co@MFI catalyst.

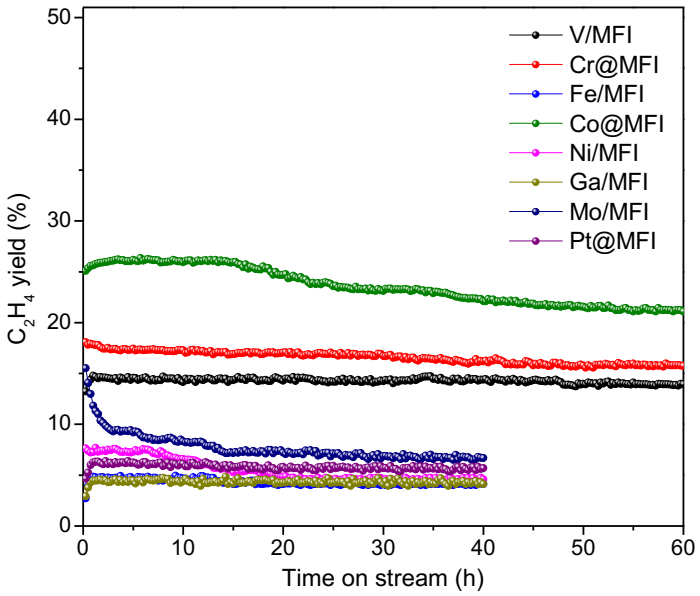

Fig. S5 Yield of C_2H_4 over different metal catalysts. Reaction conditions: 100 mg catalyst, pretreatment by 10% H_2/N_2 for 30 min, 20% C_2H_6/N_2, 10 mL/min, 1 bar, 650 °C.

Table S3. Blank test results of EDH in PID and Avantium reactors

	Pressure (bar)	C_2H_6 conversion (%)	C_2H_4 selectivity (%)
Blank	1	6.6	98.3
SiC	1	3.8	97.7
MFI	1	5.6	99.2
Blank	7.5	4.7	98.9
SiC	7.5	1.6	99.9
MFI	7.5	3.0	99.4
Reaction conditions: heating zone of the reactor was filled by SiC (for SiC), 100 mg (for MFI), 20% C_2H_6/N_2, 10 mL/min for 1 bar, 5 mL/min at 7.5 bar, 650 °C.			

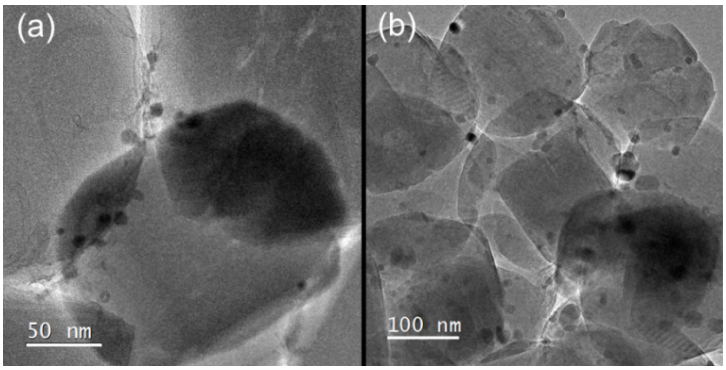

Fig. S6 TEM images of used catalysts (a) 1.3Co@MFI and (b) 2.5Co@MFI after EDHR at 1 bar.

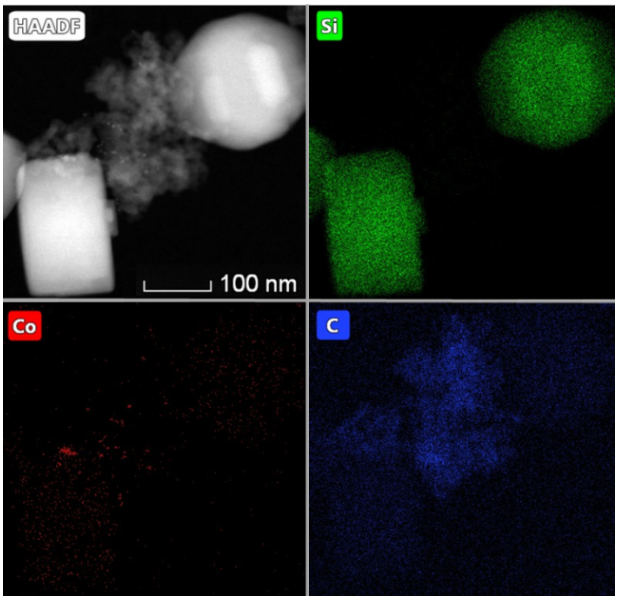

Fig. S7 STEM-HAADF image of used 0.5Co@MFI catalyst after EDH at 1 bar and elemental mappings for Si, Co, and C.

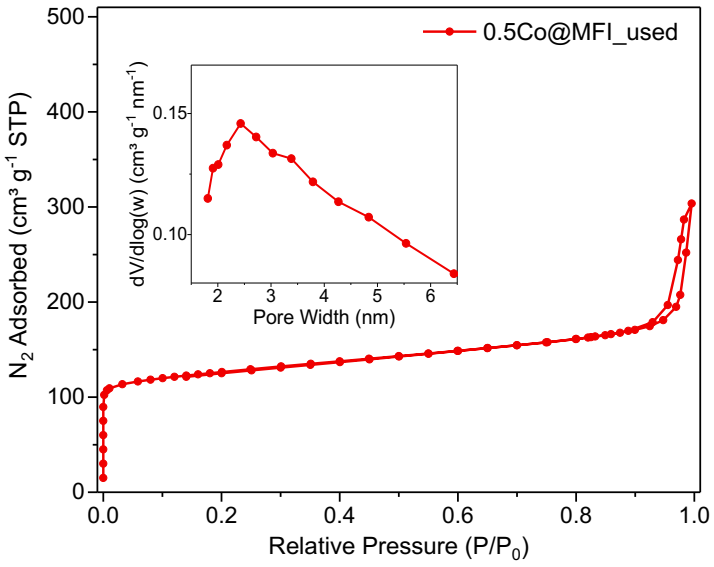

Fig. S8 Nitrogen adsorption-desorption isotherm and pore size distribution of used 0.5Co@MFI catalyst after EDHR at 1 bar.

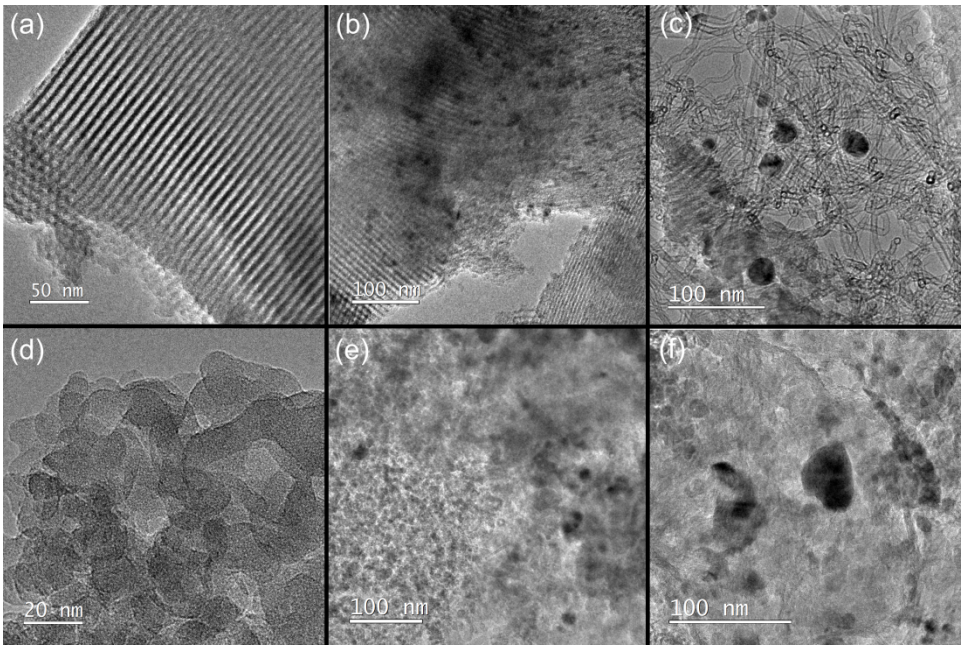

Fig. S9 TEM images of (a) fresh, (b) H_2-pretreated & (c) used 0.5Co/SBA-15 catalyst. TEM images of (d) fresh, (e) H_2-pretreated & (f) used 0.5Co/SiO_2 catalyst.

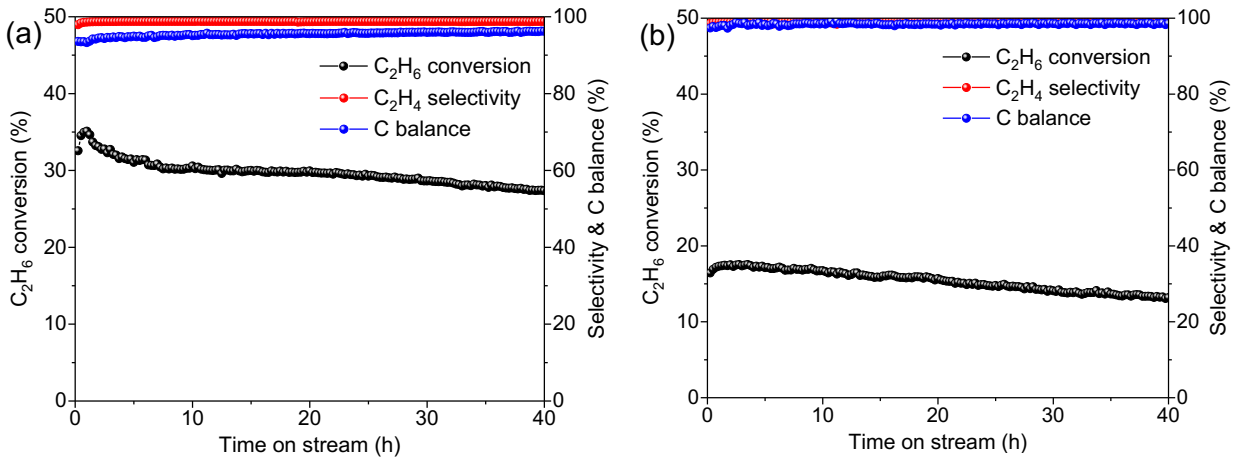

Fig. S10 Catalytic performance of 0.5Co@MFI in the non-oxidative EDHR with (a) 10% C_2H_6/N_2 and (b) 40% C_2H_6/N_2. Reaction conditions: 100 mg catalyst, pretreatment by 10% H_2/N_2 for 30 min, 10 mL/min C_2H_6/N_2, 650 °C, 1 bar.

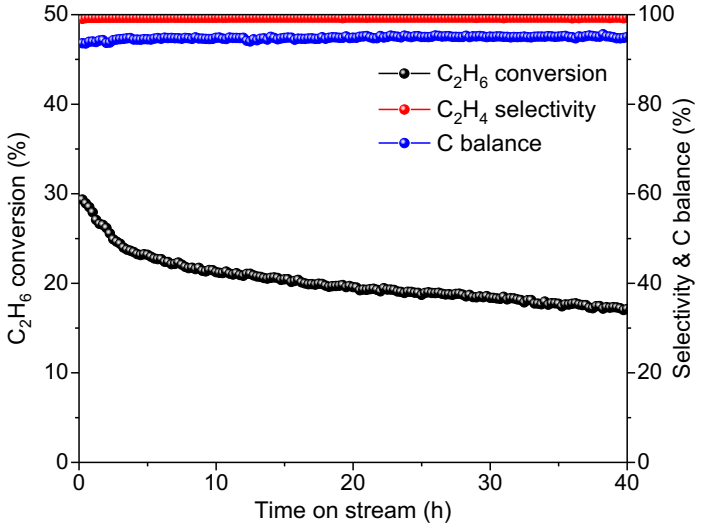

Fig. S11 Catalytic performance of 0.5Co@MFI in the non-oxidative EDHR without H_2 pretreatment. Reaction conditions: 100 mg catalyst, 20% C_2H_6/N_2, 10 mL/min, 650 °C, 1 bar.

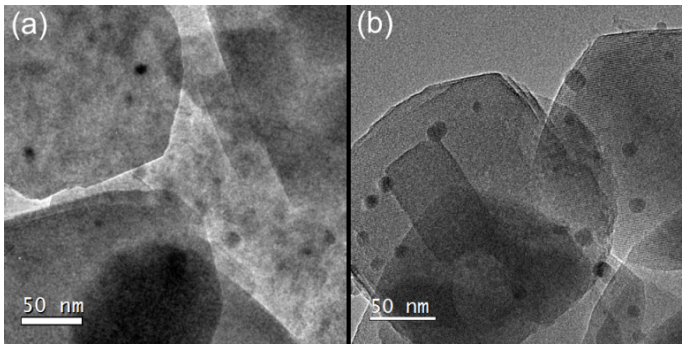

Fig. S12 TEM images of (a) uncalcined and (b) calcined 0.5Co@MFI catalysts after the 5th run of EDHR at 1 bar.

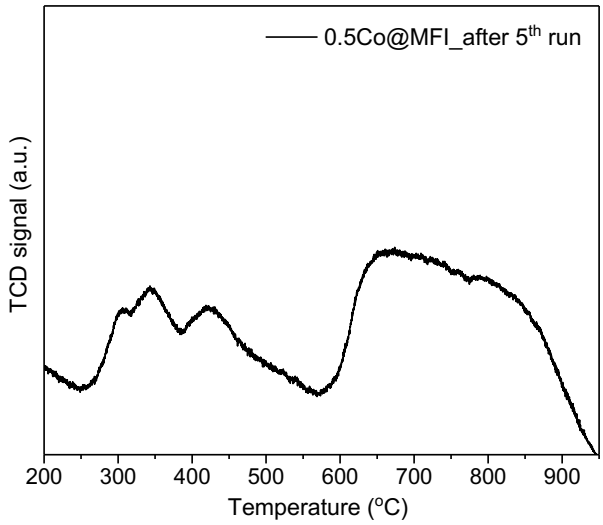

Fig. S13 H_2-TPR profile of 0.5Co@MFI catalyst after 5th run of EDHR at 1 bar. The used catalyst was regenerated in the air before performing the TPR.

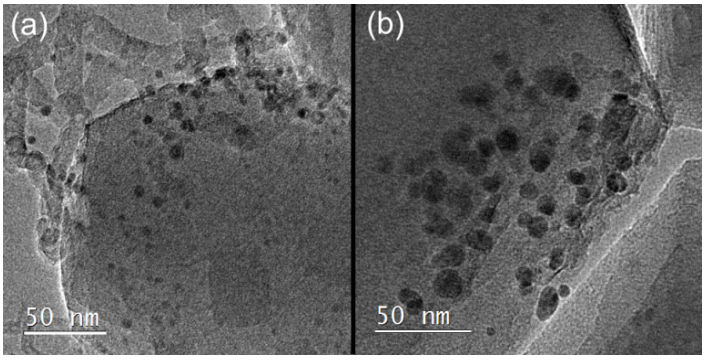

Fig. S14 TEM images of used catalysts (a) 0.5Co@MFI, & (d) 1.3Co@MFI after EDHR at 7.5 bar.

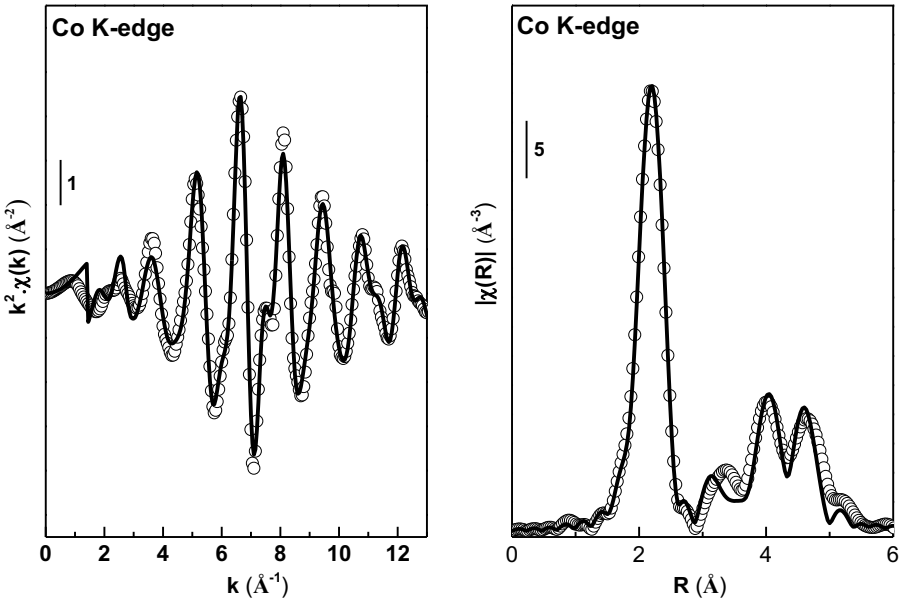

Fig. S15 Co K-edge EXAFS $k^2.\chi(k)$ function (left) and Fourier transform (right) of Co foil (uncorrected from phase-shifts). The empty circles are the experimental data while the solid lines are the fits.

Table S4. Parameters extracted from the fits of EXAFS data for Co foil

	Bond	N[a]	R [Å]	σ^2 [Å^2]	ΔE [eV]	R-factor [%]
Co foil (S_o = 0.76 ± 0.03) hcp model	Co−Co	<u>12</u>	2.49 ± 0.005	0.006 ± 0.0007	7.8 ± 0. 7	0.7
	Co−Co	<u>6</u>	3.49 ± 0.02	0.01 ± 0.003		
	Co−Co	<u>18</u>	4.35 ± 0.01	0.007 ± 0.001		
	Co−Co	<u>12</u>	4.84 ± 0.03	0.006 ± 0.006		

[a] Underlined characters denote fixed parameters.

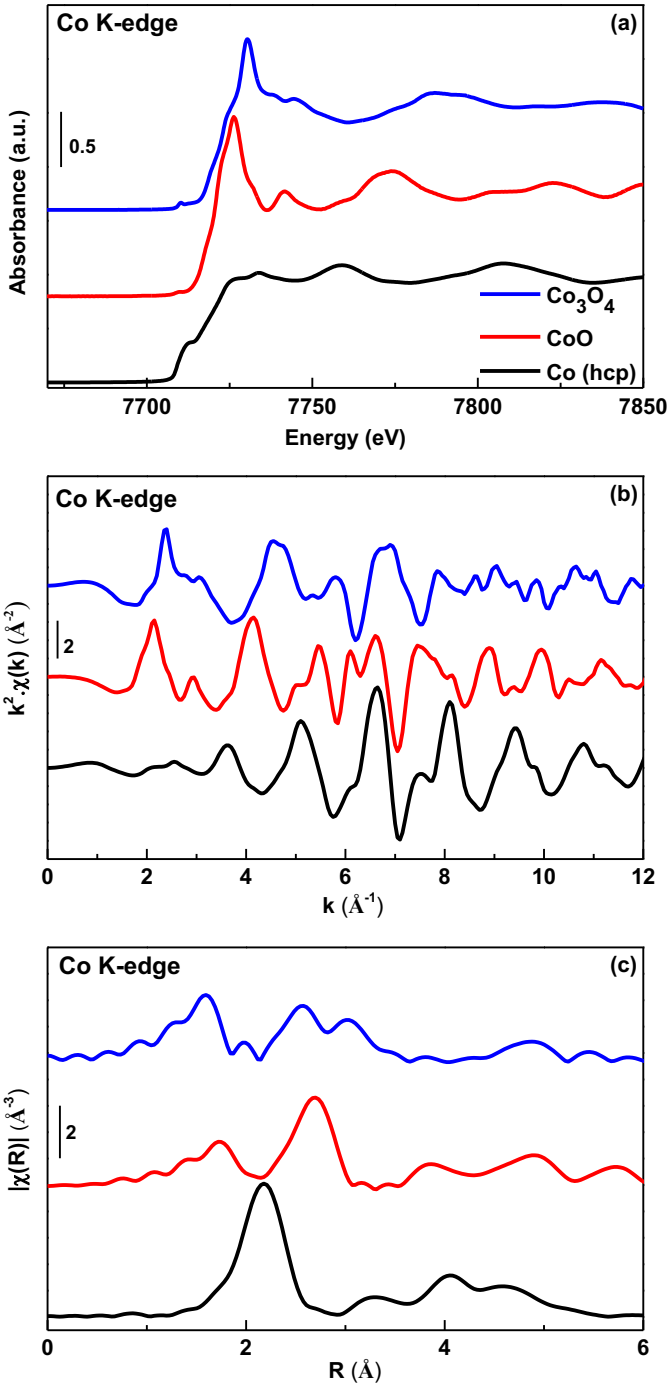

Fig. S16 (a) XANES spectra, (b) k^2 weighed EXAFS spectra, and (c) their related Fourier transforms for Co_3O_4, CoO, and Co (hcp) references at the Co K-edge.

Fig. S16a shows the XANES spectra for metallic Co, CoO, and Co_3O_4. The main features of the spectra depend on the oxidation state and the symmetry of the Co centre, especially in the pre-edge region. Co_3O_4 shows a slightly more intense pre-edge compared to CoO because 1/3 of the cobalt crystallographic sites in the Co_3O_4 crystal structure are tetrahedral.[2-4] Both cobalt oxides show an intense white line compared to the metallic Co.

The extended X-ray absorption fine structure (EXAFS) oscillations obtained from Co K-edge XAS spectra and its Fourier transform (FT) are presented in Fig. S16b and S16c. Co_3O_4 shows a spinel structure with Co^{2+} ions occupying tetrahedral sites and Co^{3+} occupying octahedral sites. The peak in the region 0.6−1.9 Å is attributed to the Co−O coordination shell for both Co^{2+} and Co^{3+} sites. The peaks in the region 1.9−3.6 Å are overlapped contributions from multiple Co−Co and Co−O scattering paths.[5] For CoO, the region 0.7−2.0 Å corresponds to the first coordination shell Co−O and the region 1.9−3.4 Å corresponds to the second coordination shell Co−Co. Finally, the spectrum of metallic Cobalt shows a main peak in the region 1.8−2.8 Å corresponding to the first coordination shell Co−Co.

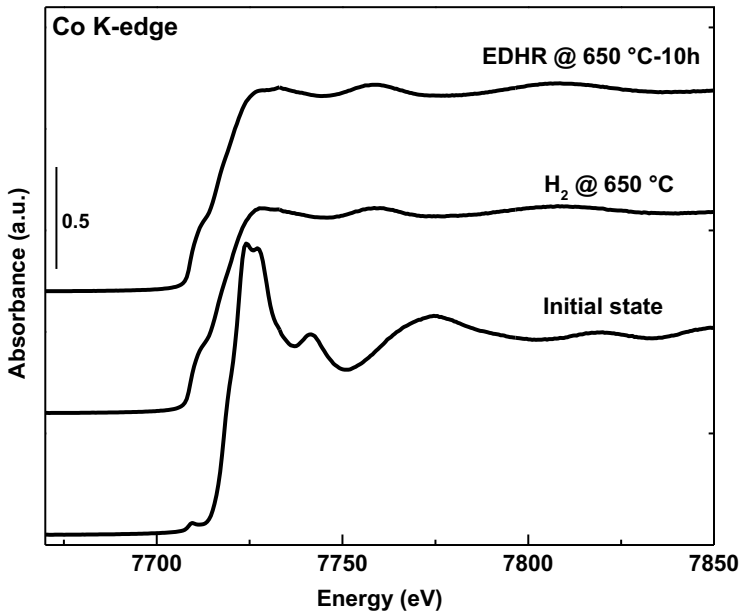

Fig. S17 Evolution of Co K-edge XANES spectra of 2.5Co@MFI at the initial state, after reduction under H_2, and after 10 h of EDHR.

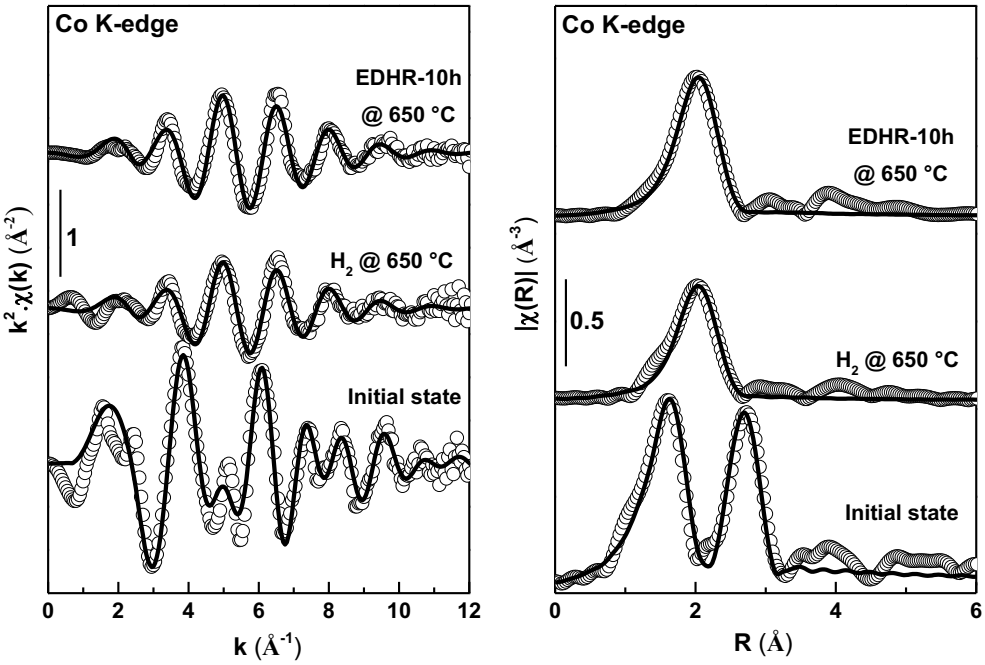

Fig. S18 k^2 weighed EXAFS spectra (left) and Fourier transforms (right) of 2.5Co@MFI at the initial state, after reduction under H_2, and after 10 h of EDHR. The empty circles are the experimental data while the solid lines are the fits.

Table S5. Parameters extracted from the fits of EXAFS data of 2.5Co@MFI at the initial state, after reduction under H_2, and after 10 h of EDHR

Conditions	Bond	N	R [Å]	σ^2 [Å^2]	ΔE [eV]	R-factor [%]
Initial state	Co−O	5.4 ± 0.7	2.08 ± 0.01	0.008 ± 0.002	1.8 ± 1.2	1.7
	Co−Co	7.7 ± 1.9	3.09 ± 0.01	0.01 ± 0.002		
H_2 @ 650°C	Co−Co	5.7 ± 1.1	2.46 ± 0.01	0.018 ± 0.002	−0.66 ± 1.5	1.2
EDHR @ 650 °C-10h	Co−Co	7.3 ± 0.8	2.46 ± 0.008	0.018 ± 0.001	−0.59 ± 0.8	0.6

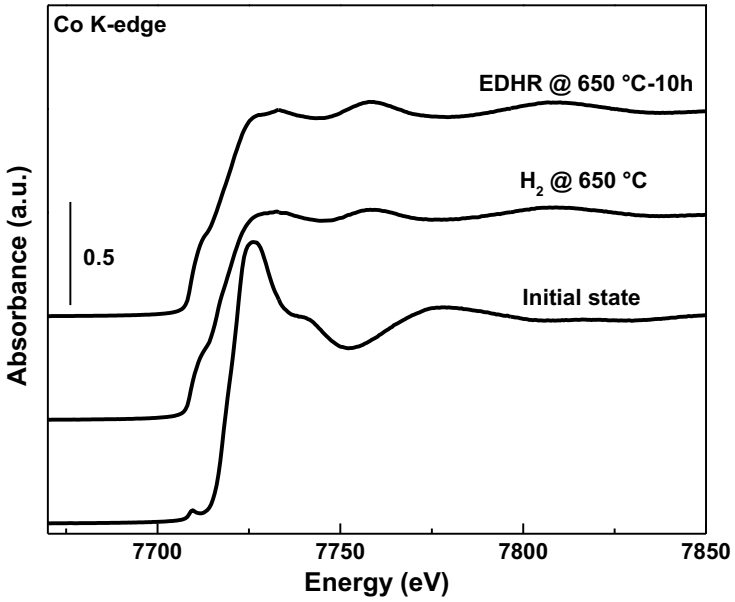

Fig. S19 Evolution of Co K-edge XANES spectra of 0.5Co/SiO_2 at the initial state, after reduction under H_2, and after 10 h of EDHR.

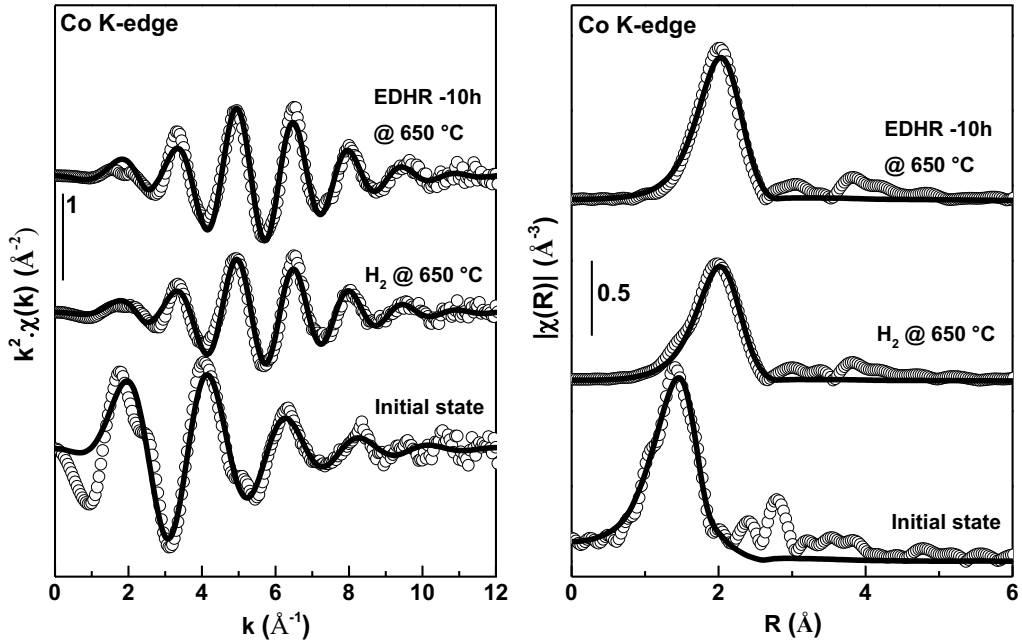

Fig. S20 k^2 weighed EXAFS spectra (left) and Fourier transforms (right) of 0.5Co/SiO_2 at the initial state, after reduction under H_2, and after 10 h of EDHR.

Table S6. Parameters extracted from the fits of EXAFS data of 0.5Co/SiO_2 at the initial state, after reduction under H_2, and after 10 h of EDHR

Conditions	Bond	N	R [Å]	σ^2 [Å^2]	ΔE [eV]	R-factor [%]
Initial state	Co−O	5.2 ± 0.36	1.98 ± 0.01	0.013 ± 0.002	−0.14 ± 0.7	2.1
H_2 @ 650 °C	Co−Co	6.9 ± 1.1	2.45 ± 0.01	0.018 ± 0.002	−2.2 ± 1.2	1.6
EDHR @ 650 °C-10h	Co−Co	9.5 ± 1.2	2.46 ± 0.01	0.019 ± 0.002	−1.36 ± 0.9	1.9

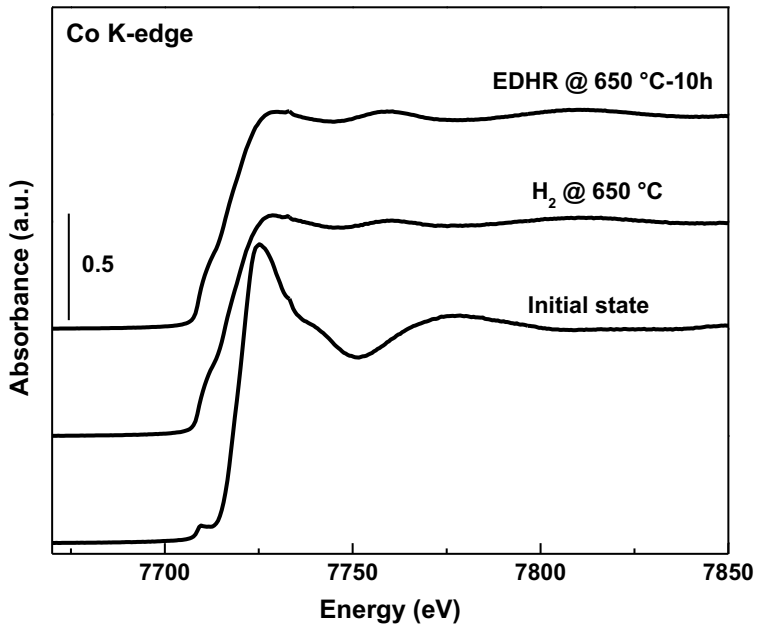

Fig. S21 Evolution of Co K-edge XANES spectra of 0.5Co/MFI at the initial state, after reduction under H_2, and after 10 h of EDHR.

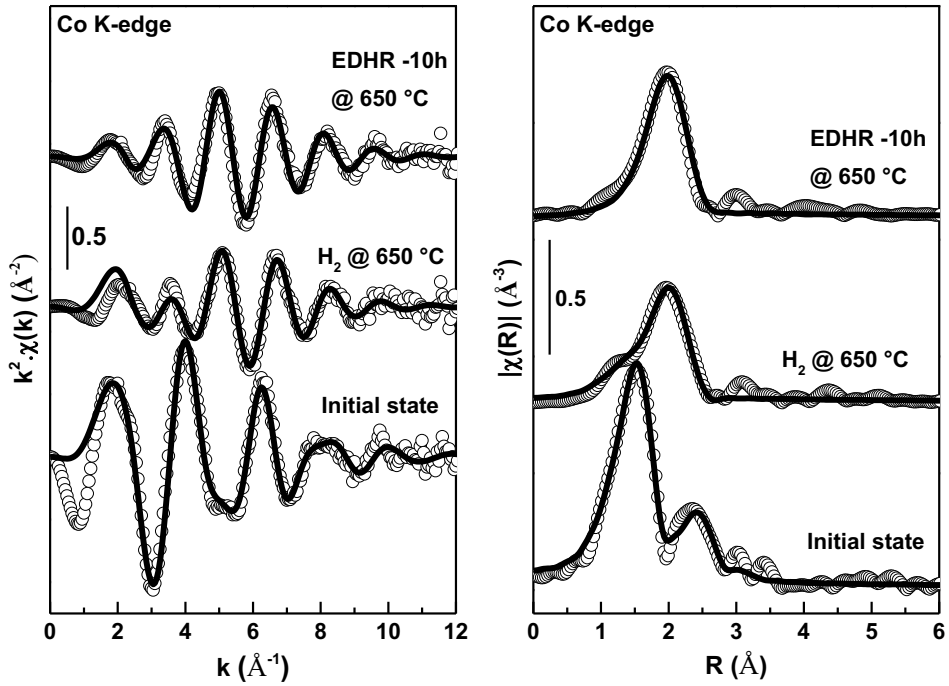

Fig. S22 k^2 weighed EXAFS spectra (left) and Fourier transforms (right) of 0.5Co/MFI at the initial state, after reduction under H_2, and after 10 h of EDHR.

Table S7. Parameters extracted from the fits of EXAFS data of 0.5Co/MFI at the initial state, after reduction under H_2, and after 10 h of EDHR

Conditions	Bond	N	R [Å]	σ^2 [Å^2]	ΔE [eV]	R-factor [%]
Initial state	Co−O	4.6 ± 0.6	2.01 ± 0.01	0.01 ± 0.002	−0.17 ± 1.1	1.3
	Co−Co	5.9 ± 3.8	3.01 ± 0.02	0.02 ± 0.008		
H_2 @ 650 °C	Co−O	1.4 ± 1.2	1.9 ± 0.02	0.02 ± 0.001	−2.9 ± 1.9	1
	Co−Co	5 ± 0.8	2.42 ± 0.01	0.019 ± 0.002		
EDHR @ 650 °C-10h	Co−Co	5.9 ± 1.5	2.43 ± 0.02	0.019 ± 0.003	−2.8 ± 1.5	1.9

Table S8. Parameters extracted from the fits of EXAFS data of 0.5Co@MFI at the initial state, after pretreatment, and after 10 h of EDHR

Conditions	Bond	N	R [Å]	σ^2 [Å^2]	ΔE [eV]	R-factor [%]
Initial state	Co−O	5 ± 0.5	2.07 ± 0.01	0.008 ± 0.002	1 ± 0.9	2.3
	Co−Co	7.7 ± 2.3	3.08 ± 0.01	0.01 ± 0.003		
H_2 @ 650 °C	Co−O	1.5 ± 0.7	1.9 ± 0.01	0.02 ± 0.009	2 ± 1.5	1
	Co−Co	4.9 ± 0.6	2.45 ± 0.01	0.018 ± 0.001		
EDHR @ 650 °C-10h	Co−Co	5.6 ± 1.2	2.45 ± 0.01	0.016 ± 0.003	2.7 ± 1.3	2.1
He @ 650 °C	Co−O	1.3 ± 0.2	1.8 ± 0.01	0.01 ± 0.003	0.2 ± 1.2	1.8
	Co−Co	1.9 ± 0.6	2.46 ± 0.01	0.015 ± 0.003		
EDHR @ 650 °C-10h	Co−O	0.9 ± 0.1	1.8 ± 0.01	0.007 ± 0.002	3.8 ± 0.7	0.2
	Co−Co	5.3 ± 0.4	2.45 ± 0.01	0.017 ± 0.0009		

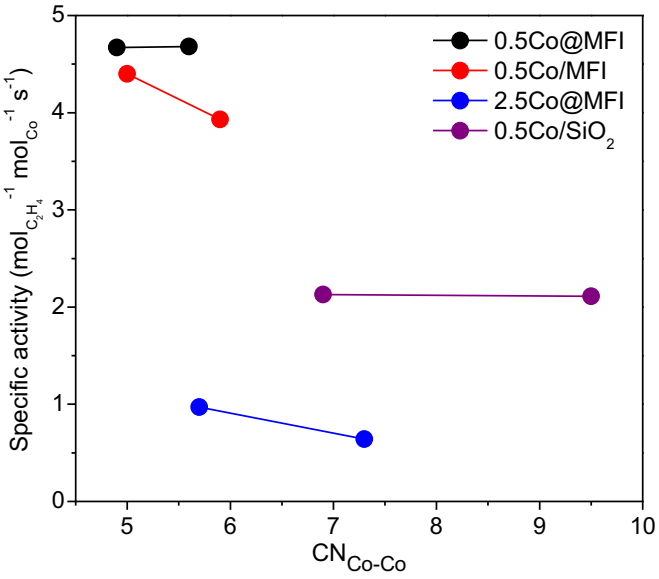

Fig. S23 The plot of specific activity vs. first shell Co−Co coordination number at the initial stage (i.e., after H_2 pretreatment) and after 10 h of EDHR for different Co-based catalysts.

Table S9. Comparison of performance and stability of our present catalyst with the earlier reported catalysts for the non-oxidative EDHR

Catalyst	Reaction conditions	Highest activity	Deactivation	Reference
10Fe/ZSM-5	0.1 g, 3240 mL h^{-1} g^{-1}, 600 °C	X = 21.8%, S = 71.6%	23% (after 4.5 h)	6
2Fe/ZSM-5	0.1 g, 3240 mL h^{-1} g^{-1}, 600 °C	X = 15.0%, S = 68.8%	12% (after 4.5 h)	6
2Zn/ZSM-5	0.1 g, 3240 mL h^{-1} g^{-1}, 600 °C	X = 35.4%, S = 68.0%	53% (after 4.5 h)	6
2Ga/ZSM-5	0.1 g, 3240 mL h^{-1} g^{-1}, 600 °C	X = 7.5%, S = 44.9%	8% (after 4.5 h)	6
In-CHA (In/Al = 0.8)	0.1 g, 600 mL h^{-1} g^{-1}, 660 °C	X = 27.2%, S = 96.9%	2.2% (after 90 h)	7
4Co/ZSM-5	0.2 g, 270 mL h^{-1} g^{-1}, 650 °C	X = 54.5%, S = 87.8%	19.6% (after 6 h)	8
0.088Pt/M-TS-1 (EA)	0.1 g, 300 mL h^{-1} g^{-1}, 600 °C	X = 16.5%, S = 98.0%	4.2% (after 6 h)	9
6Cr/γ-Al_2O_3	0.5 g, 1200 mL h^{-1} g^{-1}, 650 °C	X = 30.7%, S = 78.6%	34% (after 1 h)	10
0.5Co@MFI	0.1 g, 1200 mL h^{-1} g^{-1}, 650 °C	X = 25.7%, S = 99.6%	13.2% (after 40 h)	This work

X denotes the C_2H_6 conversion and S denotes the C_2H_4 selectivity

References

1. I. Barin, *Thermochemical Data of Pure Substances*, Wiley, 3rd edn., 1995.
2. A. Moen, D. G. Nicholson, M. Rnning, G. M. Lamble, J.-F. Lee and H. Emerich, *J. Chem. Soc., Faraday Trans.*, 1997, 93, 4071-4077.
3. A. Moen, D. G. Nicholson, B. S. Clausen, P. L. Hansen, A. Molenbroek and G. Steffensen, *Chem. Mater.*, 1997, 9, 1241-1247.
4. G. Jacobs, Y. Ji, B. H. Davis, D. Cronauer, A. J. Kropf and C. L. Marshall, *Appl. Catal. A: Gen.*, 2007, 333, 177-191.
5. A. Griboval-Constant, A. Butel, V. V. Ordomsky, P. A. Chernavskii and A. Y. Khodakov, *Appl. Catal. A: Gen.*, 2014, 481, 116-126.
6. L.-C. Wang, Y. Zhang, J. Xu, W. Diao, S. Karakalos, B. Liu, X. Song, W. Wu, T. He and D. Ding, *Appl. Catal. B: Environ.*, 2019, 256, 117816.
7. Z. Maeno, S. Yasumura, X. Wu, M. Huang, C. Liu, T. Toyao and K.-i. Shimizu, *J. Am. Chem. Soc.*, 2020, 142, 4820-4832.
8. H. Guo, C. Miao, W. Hua, Y. Yue and Z. Gao, *Microporous Mesoporous Mater.*, 2021, 312, 110791.
9. Y. Pan, A. Bhowmick, W. Wu, Y. Zhang, Y. Diao, A. Zheng, C. Zhang, R. Xie, Z. Liu, J. Meng and D. Liu, *ACS Catal.*, 2021, 11, 9970-9985.
10. H. Yang, L. Xu, D. Ji, Q. Wang and L. Lin, *React. Kinet. Catal. Lett.*, 2002, 76, 151-159.